

# MAGNETIC STRESS AT THE MARGINALLY STABLE ORBIT: ALTERED DISK STRUCTURE, RADIATION, AND BLACK HOLE SPIN EVOLUTION

ERIC AGOL

Department of Physics and Astronomy, Johns Hopkins University, Baltimore, MD 21218, agol@pha.jhu.edu

AND

JULIAN H. KROLIK

Department of Physics and Astronomy, Johns Hopkins University, Baltimore, MD 21218, jhk@pha.jhu.edu

*Draft version November 17, 2021*

## ABSTRACT

Magnetic connections to the plunging region can exert stresses on the inner edge of an accretion disk around a black hole. We recompute the relativistic corrections to the thin-disk dynamics equations when these stresses take the form of a time-steady torque on the inner edge of the disk. The additional dissipation associated with these stresses is concentrated relatively close outside the marginally stable orbit, scaling as  $r^{-7/2}$  at large radius. As a result of these additional stresses: spin-up of the central black hole is retarded; the maximum spin-equilibrium accretion efficiency is 36%, and occurs at  $a/M = 0.94$ ; the disk spectrum is extended toward higher frequencies; line profiles (such as Fe K $\alpha$ ) are broadened if the line emissivity scales with local flux; limb-brightening, especially at the higher frequencies, is enhanced; and the returning radiation fraction is substantially increased, up to 58%. This last effect creates possible explanations for both synchronized continuum fluctuations in AGN, and polarization rises shortward of the Lyman edge in quasars. We show that no matter what additional stresses occur, when  $a/M < 0.36$ , the second law of black hole dynamics sets an absolute upper bound on the accretion efficiency.

*Subject headings:* accretion, accretion disks — black hole physics — galaxies: active — line profiles — polarization — relativity

## 1. INTRODUCTION

Early work on black hole accretion disks pointed out the possibility that magnetic stresses might exert a torque on the inner parts of the accretion disk (Page & Thorne 1974, Thorne 1974, Ruffini & Wilson 1975, King & Lasota 1977). However, in virtually every recent account of the dynamics of accretion disks around black holes, it has been assumed that there is no stress at the disk’s inner edge, which should occur very close to the radius of the marginally stable orbit,  $r_{ms}$ . That this should be so was variously argued on the basis that the plunging matter in the region of unstable orbits has too little inertia to affect the disk, or rapidly becomes causally disconnected from the disk, or that such stresses were due to relatively weak transport processes that could not compete with the large gravitational forces pulling matter away from the disk. Recently this view has been questioned (Krolik 1999) on the basis that magnetic fields are the likely agent of torque in accretion disks (Balbus & Hawley 1998). If this is so, and their strength in the plunging region is what would be expected on the basis of flux-freezing, they should be strong enough in that zone to both make the Alfvén speed relativistic (postponing the point of causal decoupling) and exert forces competitive with gravity.

If matter inside the marginally stable orbit does, indeed, remain magnetically connected to the disk, it can exert a sizable torque on the the portion of the disk containing the field-line footpoints. Gammie (1999) has shown that, within the confines of a highly-idealized model of inflow dynamics, this torque can considerably enhance the amount

of energy released in the disk.

In fact, even if there were no continuing accretion, field lines attached to the event horizon of a spinning black hole and running through the disk could exert torques of a very similar character (Blandford 1998, D.M. Eardley, private communication). We will call this situation the “infinite efficiency limit.”

A corollary of torque on the inner edge of the disk is an increase in the outward angular momentum flux. In a time-steady state, this additional angular momentum flux must be conveyed by additional stress. Additional local dissipation must accompany the additional stress. It is the principal object of this paper to compute how this dissipation is distributed through the disk, and examine the consequences for observable properties.

Time-steady torques at  $r_{ms}$  are not the only way that energy may be transmitted from the plunging region to the disk—the torque may be variable, it may be delivered over a range of radii, and there may be radial forces exerted that carry no angular momentum. However, in this paper, we will restrict our attention to this simplest possible case.

## 2. THE RELATIVISTIC CORRECTION FACTORS

### 2.1. Dissipation as a function of radius

Novikov & Thorne (1973) and Page & Thorne (1974) showed how the surface brightness and vertically-integrated stress in the fluid frame for a time-steady, geometrically thin, relativistic accretion disk could be written as the Newtonian forms multiplied by correction factors

that approach unity at large radius. In the notation of Page & Thorne (1974), conservation of angular momentum is given by

$$\frac{\partial}{\partial r} \left( L^\dagger + \frac{C^{1/2}}{B\partial\Omega/\partial r} f \right) = L^\dagger f, \quad (1)$$

where  $r$  is the Boyer-Lindquist radial coordinate,  $L^\dagger$  is the conserved specific angular momentum of a circular orbit at radius  $r$ ,  $f$  is a function of radius defined such that the flux at the disk surface in the fluid frame  $F = \dot{M}_o f / (4\pi r)$ , and  $\dot{M}_o$  is the rest-mass accretion rate. As usual,  $\Omega$  is the angular frequency of a circular orbit at radius  $r$ . We also follow Novikov & Thorne (1973) by defining four auxiliary functions:

$$B(x) = 1 + a_*/x^{3/2} \quad (2)$$

$$C(x) = 1 - 3/x + 2a_*/x^{3/2} \quad (3)$$

$$D(x) = 1 - 2/x + a_*^2/x^2 \quad (4)$$

$$F(x) = 1 - 2a_*/x^{3/2} + a_*^2/x^2, \quad (5)$$

with  $x$  the radius in units of  $r_g = GM/c^2$  and  $a_*$  the dimensionless black hole spin parameter. In the usual approach, the boundary condition on  $f$  at the radius  $r_{ms}$  of the marginally stable orbit is  $f_{ms} = 0$ . The appropriate boundary condition when there is non-zero stress at  $r_{ms}$  is

$$f_{ms} = \frac{3}{2} \frac{\Delta\epsilon}{x_{ms} C_{ms}^{1/2}}, \quad (6)$$

where  $C_{ms} = C(r_{ms})$ , and  $\Delta\epsilon$  is the additional radiative efficiency relative to the one computed in terms of the binding energy at  $r_{ms}$ ,  $\epsilon_0$ , so that  $\epsilon = \Delta\epsilon + \epsilon_0$ . This choice of  $f_{ms}$  ensures that the integrated additional dissipation matches  $\Delta\epsilon$ , and corresponds to a stress

$$W_\phi^r(r_{ms}) = \frac{\Delta\epsilon \dot{M}_o}{2\pi r_{ms} \Omega_{ms}}. \quad (7)$$

We refer to a disk with  $\Delta\epsilon = 0$  as a ‘‘Novikov-Thorne disk.’’

Using this boundary condition, the locally generated surface flux becomes

$$F(x) = \frac{3}{8\pi} \frac{GM\dot{M}_o}{r^3} \left[ \frac{x_{ms}^{3/2} C_{ms}^{1/2} \Delta\epsilon}{C(x)x^{1/2}} + R_R^{NT}(x) \right] \quad (8)$$

where  $R_R^{NT}(x)$  is the expression found by Novikov & Thorne (1973). The standard relativistic correction factor  $R_R^{NT}$  goes to zero as  $x$  approaches  $x_{ms}$  from above, so that  $F$  (when the inner-edge stress is zero) peaks well outside the marginally stable orbit. By contrast, the additional dissipation due to a torque on the inner edge is concentrated very close to  $r_{ms}$ , and is non-zero at the inner edge. The degree of concentration can be quantified by measuring  $r_{1/2}$ , the radius within which fifty percent of the radiation is emitted: the half-light radius is a factor of a few smaller for torque-driven flux than for Novikov-Thorne flux. Figure 1 shows the half-light radius for a Novikov-Thorne disk,  $r_{1/2}^0$ , and an infinite-efficiency disk,  $r_{1/2}^\infty$ , as a function of  $a_*$ .

In the limit of infinite efficiency or zero accretion rate,  $\dot{M}_o\epsilon$  remains finite, so the first term in equation [8] dominates; in this case, the flux scales as  $r^{-7/2}$  at large  $r$  rather than as  $r^{-3}$  as in the standard thin disk. The expression for the surface flux becomes:

$$F^{(\infty)}(x) = \frac{3}{2} \frac{c^3}{r_g \kappa_T x^{7/2}} \frac{L}{L_{Edd}} \frac{x_{ms}^{3/2} C_{ms}^{1/2}}{C(x)}, \quad (9)$$

where  $L_{Edd}$  is the Eddington luminosity and  $\kappa_T$  is the Thomson opacity per unit mass.

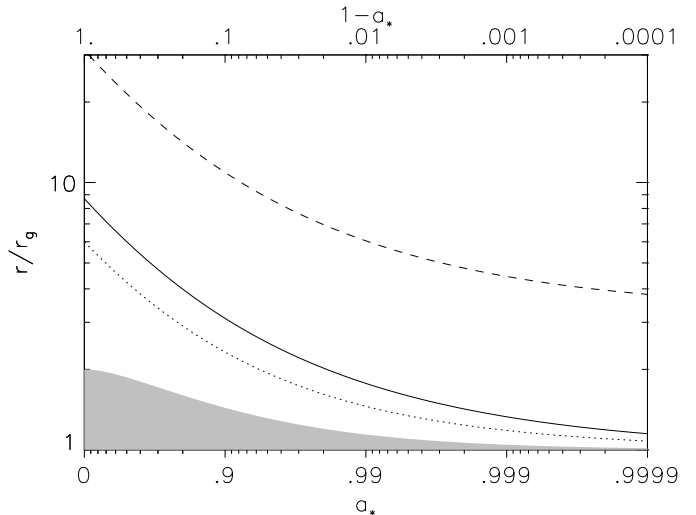


Fig. 1. Half-light radii for the Novikov-Thorne disk (dashed line) and infinite-efficiency disk (solid line). Also plotted are  $r_{ms}$  (dotted line) and the region inside the horizon (shaded).

The angular momentum conservation equation corresponding to equation [8] is

$$- \int dz T_{r\phi}(z) = \frac{\dot{M}_o \Omega_K(x)}{2\pi} \left[ \frac{x_{ms}^{3/2} C_{ms}^{1/2} \Delta\epsilon}{D(x)x^{1/2}} + R_T^{NT}(x) \right], \quad (10)$$

where  $R_T^{NT}$  is the torque correction factor (Novikov & Thorne 1973, Page & Thorne 1974) in the notation of Krolik (1999).

To clarify the meaning of the extra dissipation, we will write down equation [8] pretending that gravity is purely Newtonian:

$$F^{(N)}(r) = \frac{3}{8\pi} \frac{GM\dot{M}_o}{r^3} \left[ \Delta\epsilon \sqrt{\frac{r_{in}}{r} \frac{r_{in}}{r_g}} + \left( 1 - \sqrt{\frac{r_{in}}{r}} \right) \right], \quad (11)$$

where  $r_{in}$  is the disk inner edge. The first term in the bracket is the usual Shakura-Sunyaev (1973) correction factor, while the second term is derived from the extra torque at the inner edge. This equation (actually first derived by Popham & Narayan 1993) never applies in the relativistic case, but can apply, for example, to a disk around a star where a torque is exerted by the spinning magnetosphere or through a boundary layer, or to a thin disk surrounding a different disk solution, such as an ADAF, where a torque is exerted by the flow inside the transition point.

## 2.2. Returning radiation

To find the surface brightness distribution of the disk as seen by distant observers, it is necessary first to correct the intrinsic surface brightness due to local dissipation for the additional energy supplied by photons originally emitted at a different radius, but returned to the disk by gravity. In the conventional picture, this is a small correction (Cunningham 1976). Here, however, because so much more of the energy is released deep in the relativistic potential, it can be a much greater effect.

To compute the additional returning radiation, we followed the method developed by Cunningham (1976), with a few modifications. The numerical method is described in Agol (1997). We compute the flux transfer function,  $T_f$ , by following photons emitted from each radius that return to the accretion disk, assuming the disk surface is flat and the radiation is isotropic in the fluid frame. We ignore the stress carried by these photons (i.e., we set  $T_s = 0$  in Cunningham's parlance). We also assume that any radiation that returns to the disk inside  $r_{ms}$  is captured by the black hole—this radiation will be advected or scattered inwards by the inflowing gas, which has a large inward radial velocity. Finally, we (temporarily) assume (as does Cunningham) that the radiation returning to the disk is absorbed and thermalized before being reemitted; this assumption is probably not appropriate in practice, but greatly simplifies computation of the transfer function since in this approximation  $T_f$  is independent of frequency. We will discuss later how breaking this assumption may change the spectrum.

In Figure 2a, we plot versus radius the fraction of emitted radiation which returns to the disk outside  $r_{ms}$ , which enters the black hole or returns to the disk inside  $r_{ms}$ , and which reaches infinity directly, for the cases  $a_* = 0.9999$  and  $a_* = 0$ . The fraction reaching infinity and returning to the disk are nearly independent of the black hole spin. The fraction returning to the disk is greater than 10% for  $r \lesssim 6r_g$ , so when the emitted energy is concentrated inside this radius (see figure 1), then returning radiation will play an important role in modifying disk spectra. For  $r \lesssim 1.5r_g$ , less than half of the radiation reaches infinity directly - most returns to the disk. For  $a_* = 0$ , the fraction of radiation which is captured by the black hole or returns inside  $r_{ms}$  increases since  $r_{ms}$  is so large; this fraction never exceeds 8%.

The fraction of returning radiation integrated over all radii,  $f_{ret}$  (as measured at infinity), is shown (as a function of  $a_*$ ) in Figure 2b (dashed lines) for two limiting efficiencies:  $\epsilon = \epsilon_0$  ( $f_{ret}^0$ ) and  $\epsilon = \infty$  ( $f_{ret}^\infty$ ). The fraction for any other efficiency can be found by taking a linear combination of the fraction for these two efficiencies

$$f_{ret} = (f_{ret}^0 \epsilon_0 + f_{ret}^\infty \Delta\epsilon) / \epsilon. \quad (12)$$

As can be seen from the figure,  $f_{ret}$  is relatively small for  $a_* = 0$ , even for  $\epsilon = \infty$ . However,  $f_{ret}$  grows quickly with increasing  $a_*$ . The primary reason for this is that  $r_{ms}$  shrinks with increasing  $a_*$ , so that relativistic effects on the photon trajectories become more important. Trajectory curvature is especially strong for those photons coming from small radii whose initial direction would carry them over the black hole. When  $a_*$  and  $\Delta\epsilon$  are comparatively large, up to 58% of the energy due to the extra

dissipation ends up striking the disk.

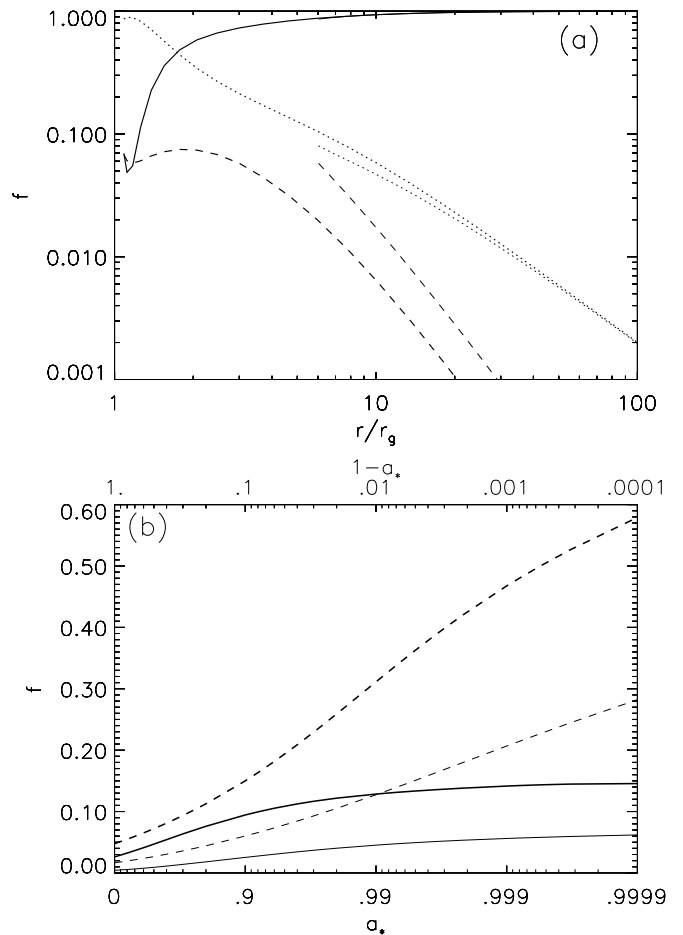


Fig. 2. (a) Fraction of locally emitted flux which reaches infinity (solid lines), returns to the disk (dotted lines), and enters the black hole or returns inside  $r_{ms}$  (dashed lines) versus radius. The heavy lines are for  $a_* = 0.9999$  and the lighter lines for  $a_* = 0$ . (b) Fraction of energy that returns to accretion disk integrated over radius (dashed lines) or that is absorbed by the black hole (solid lines) as a function of spin. The heavy lines are for an infinite efficiency disk, while the lighter lines are for a Novikov-Thorne disk.

The enhanced dissipation near  $r_{ms}$  also leads to an increase in the fraction of captured photons. We have computed this fraction integrated over all radii,  $f_{BH}$ , using the same general relativistic transfer code just described. Our results for this effect are also illustrated in Figure 2b, again for  $\epsilon = \epsilon_0, \infty$ . The  $\epsilon = \epsilon_0$  results agree with Thorne (1974). Equation [12] applies to  $f_{BH}$  as well. The fraction of locally generated radiation that ultimately escapes from the disk to infinity is simply  $f_{esc} \equiv 1 - f_{BH}$ . Radiation that returns to the accretion disk we assume is reradiated isotropically and locally, and thus eventually reaches infinity or the black hole. We fold these multiply reprocessed photons into the final result. The nominal accretion efficiency,  $\epsilon$ , is then multiplied by  $f_{esc}$  to find the actual radiative efficiency of the flow. The largest  $f_{BH}$  is 0.15, achieved for  $\epsilon \rightarrow \infty$  and  $a_* \rightarrow 1$ .

The black hole bends the radiation back to the disk so

that an observer on the disk sees the far side of the disk as a mirage above the black hole, which peaks in brightness within a few  $r_g$  of the disk plane. The flux at large radius then scales as  $H/r^{-3}$ , where  $H$  represents the flux-weighted height of the image above the disk plane. The ratio of the returning radiation to locally generated radiation,  $R_{ret}(\epsilon, a_*, r)$ , varies as a function of radius. For a Novikov-Thorne disk,  $R_{ret}$  is infinite at  $r_{ms}$ , then decreases rapidly, asymptoting to a constant for  $r \gtrsim 10r_g$ . In the case of an infinite efficiency disk (with  $\dot{M}_o = 0$ ), the locally generated surface brightness scales as  $r^{-7/2}$  at large radius, while the returning radiation scales as  $r^{-3}$ , so  $R_{ret}$  diverges as  $r^{1/2}$  at large radius. For finite  $\Delta\epsilon$ , the returning flux may dominate at intermediate radii; however, at large radius,  $R_{ret}$  asymptotes to a constant due to the fact that for large enough radius both returning and locally generated flux scale as  $r^{-3}$ . For  $r \gtrsim 10r_{ms}$  and  $\epsilon \leq 1$ ,  $R_{ret}$  differs by at most 25% from the value at  $r = \infty$ . We computed  $R_{ret}(\epsilon, a_*, \infty)$  as a function of  $a_*$  and  $\epsilon$ ; this function is shown in Figure 3. Fitting formulae for this quantity are given in the appendix; these formulae can be used to compute the returning flux at large radius for arbitrary  $a_*, \epsilon$ . As can be seen in Figure 3, the returning radiation can be a significant fraction of the locally generated radiation, and may therefore be important for construction of disk atmospheres. Returning radiation can also lead to significant fluctuations on the light-crossing time, as discussed in §3.3.

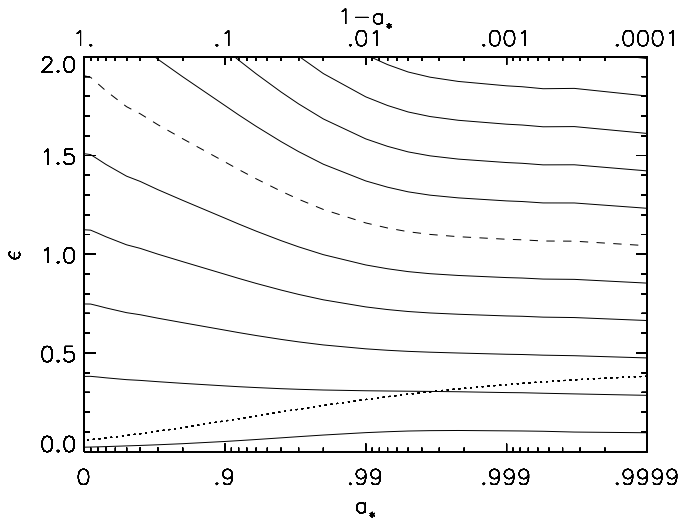


Fig. 3. Contour plot of  $R_{ret}$  at large radius. Solid contours are shown with spacing of 0.2, from  $R_{ret} = 0$  at the bottom to  $R_{ret} = 1.8$  at the top. The dotted line is  $\epsilon_0$ ; the dashed line is the contour of  $R_{ret} = 1$ .

### 3. CONSEQUENCES

#### 3.1. Black hole growth and spin-up (or spin-down)

Accreting matter enters the black hole with a certain amount of angular momentum, changing the spin of the black hole. When there is no stress at the marginally stable orbit, the angular momentum absorbed per unit rest mass accreted is exactly the specific angular momentum of the marginally stable orbit,  $L_{ms}^\dagger = MF_{ms}C_{ms}^{-1/2}x_{ms}^{1/2}$  (here we use conventional relativistic units in which  $G = c = 1$ ).

However, when there are stresses at  $r_{ms}$ , angular momentum is transferred from the matter inside  $r_{ms}$  to the disk. This reduces the accreted angular momentum by an amount  $\mathcal{L}_{ms}L_{ms}^\dagger$ , where

$$\mathcal{L}_{ms} = x_{ms}B_{ms}C_{ms}^{1/2}F_{ms}^{-1}\Delta\epsilon \quad (13)$$

when all the energy liberated in the plunging region is delivered to the disk in the form of work done by torque.  $\mathcal{L}_{ms} = 3\sqrt{2}\Delta\epsilon$  when  $a_* = 0$ , falling towards  $\sqrt{3}\Delta\epsilon$  when  $a_*$  approaches one. Thus, the rate at which black holes are spun up is substantially reduced relative to what would be expected in the conventional picture. Surprisingly, even when the black hole is initially spinless, it can be spun backwards when  $\epsilon > 1 - 1/\sqrt{2} \sim 0.29$ !

Considerations of black hole spin-up also place an upper bound on the possible increase in efficiency due to torques on the disk. By the second law of black hole dynamics, the area,  $A$ , of the black hole must increase with time; that is,

$$\frac{dA}{dt} = \frac{\partial A}{\partial M} \frac{dM}{dt} + \frac{\partial A}{\partial J} \frac{dJ}{dt} > 0. \quad (14)$$

Since  $dM/dt$  and  $dJ/dt$  both depend on  $a_*$  and  $\epsilon$ , this constraint can be changed into a constraint on  $\epsilon$  as a function of  $a_*$ . For  $a_* < 0.3584$ , there is a maximum achievable efficiency

$$\epsilon_{max} = 1 - \frac{a_*C_{ms}^{1/2}x_{ms}^{3/2}}{a_*^2 + a_*x_{ms}^{3/2} - 2(1 + \sqrt{1 - a_*^2})}. \quad (15)$$

Note that  $\epsilon_{max} = 1$  for  $a_* = 0$ , because, of course, there is no spin energy to tap. For  $a_* \simeq 0.3584$ , the denominator equals zero, so  $\epsilon_{max}$  diverges; above this critical spin, the decrease in angular momentum dominates the change in surface area, eliminating any upper bound on  $\epsilon_{max}$ . When accreted radiation is included,  $\epsilon_{max}$  increases slightly. We plot  $\epsilon_{max}$  in Figure 4.

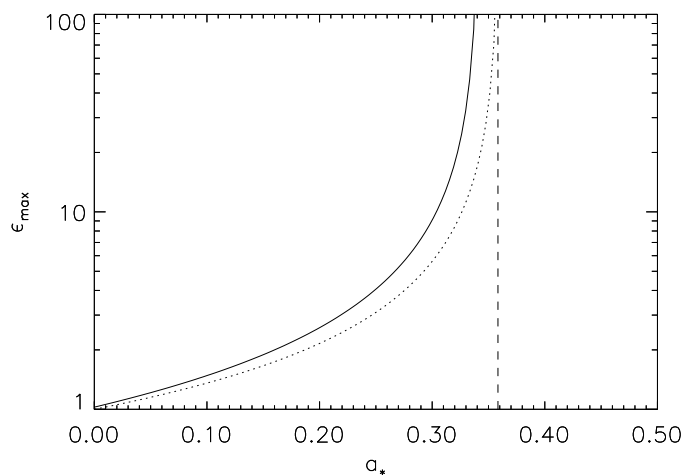


Fig. 4. Plot of the maximum achievable efficiency ( $\epsilon_{max}$ ) vs. spin due to the limit imposed by the second law of black hole dynamics with (solid) and without (dotted) the effects of radiation.

As Thorne (1974) showed, when  $a_*$  approaches one, the angular momentum of the black hole is also affected by

photon capture. Most of the photons emitted close to  $r_{ms}$  directed against the sense of black hole rotation are captured by the black hole, whereas fewer of the prograde photons fall into the hole. This extra negative angular momentum prevents it from spinning up all the way to  $a_* = 1$ . Under the assumption of isotropic radiation in the fluid frame (and, of course, zero stress at  $r_{ms}$ ), Thorne estimated that the maximum achievable  $a_* \simeq 0.998$ . To describe this effect in our context, we again normalize to  $L_{ms}^\dagger$ , so that the photon “reverse torque” per unit accreted mass is  $\mathcal{L}_\gamma \equiv -(L_{ms}^\dagger \dot{M}_o)^{-1} (dJ/dt)_{rad}$ , where the notation is adapted from Thorne (1974).

Combining the effects of mechanical torque and photon capture, we find that the net rate of change of the black hole’s angular momentum is

$$\frac{dJ}{dt} = L_{ms}^\dagger \dot{M}_o (1 - \mathcal{L}_{ms} - \mathcal{L}_\gamma). \quad (16)$$

Because both  $\mathcal{L}_\gamma$  and  $\mathcal{L}_{ms}$  depend on the state of magnetic coupling, as well as on  $a_*$ , it is no longer possible to speak of a definite upper bound on the attainable black hole spin. Rather, one can instead define the accretion efficiency,  $\epsilon_{eq}(a_*)$ , at which  $da_*/dM = 0$  for a given  $a_*$ ; for  $\epsilon > \epsilon_{eq}$ , the black hole is spun down due to accretion. To compute  $\epsilon_{eq}$ , we write  $-L_\gamma = (dJ/dt)_{rad}/(\dot{M}_o L_{ms}^\dagger) = J'_1 + \epsilon J'_1$  and  $(dM/dt)_{rad}/\dot{M}_o = M'_1 + \epsilon M'_2$  (we give fitting formulae for these functions in the appendix). Then, the equilibrium efficiency is given by:

$$\epsilon_{eq} = \frac{2a_*(1 + M'_1) - \epsilon_0 x_{ms}^{3/2} B_{ms} - L_{ms}^\dagger (1 + J'_1)}{2a_*(1 - M'_2) - x_{ms}^{3/2} B_{ms} + L_{ms}^\dagger J'_2}. \quad (17)$$

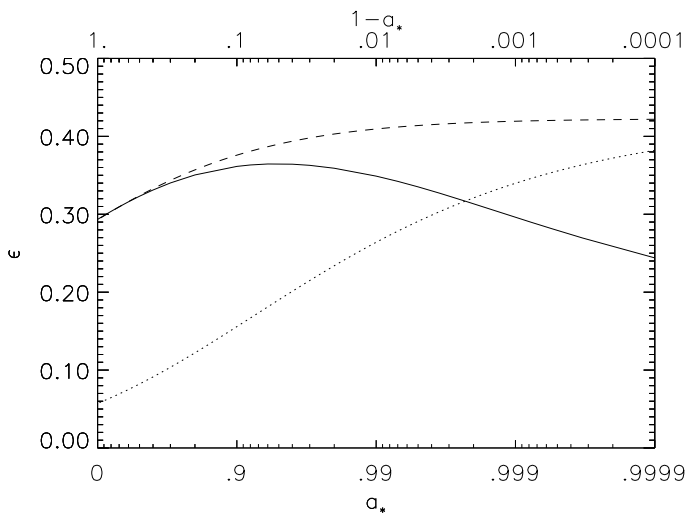


Fig. 5. Plot of  $\epsilon_{eq}$  with (solid) and without (dashed) effects of returning radiation. The dotted line is  $\epsilon_0$ , the Novikov & Thorne efficiency.

Figure 5 shows  $\epsilon_{eq}(a_*)$  when only magnetic and matter torques are included (dashed line), and when magnetic, matter, and radiation torques are included (solid line), as well as  $\epsilon_0(a_*)$ , the efficiency of accretion (not in equilibrium) when magnetic torques are ignored (dotted line). When accreted radiation is ignored, equation [17] simplifies to:

$$\epsilon_{eq} = 1 - \frac{\sqrt{C_{ms}}}{2 - B_{ms}}. \quad (18)$$

This limit is accurate for  $a_* < 0.5$ , and only creates a significant error for  $a_* > 0.9$ , for the radiation torque is unimportant when the spin is relatively small. Some interesting limiting values are  $\epsilon_{eq}(0) = 1 - 1/\sqrt{2}$ , and, when radiation effects are ignored,  $\epsilon_{eq}(1) = 1 - 1/\sqrt{3}$ , which equals  $\epsilon_0(1)$ . However, when the radiation torque is included,  $\epsilon_{eq}$  is significantly reduced for  $a_* > 0.9$ , and  $\epsilon_{eq} < \epsilon_0$  for  $a_* > 0.998$ , the same maximum spin found by Thorne (1974). The maximum equilibrium efficiency is 0.36, and occurs at  $a_* = 0.94$ .

A variety of spin histories is possible in this picture, for the efficiency is controlled jointly by the strength of the magnetic torques and the black hole spin. If the torque on the disk is always positive, the region below the curve  $\epsilon_0(a_*)$  in figure 5 is unreachable. In that case,  $a_* = 0.998$  would still be the maximum spin achievable by accretion, although other spin-up mechanisms, such as black hole mergers or non-magnetic accretion, might permit this limit to be exceeded.

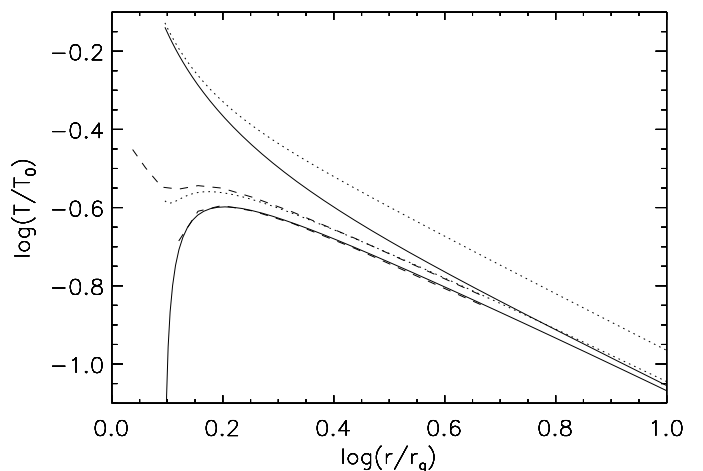


Fig. 6. Plot of the effective temperature vs. radius for a black hole with  $a_* = 0.998$ . The temperature is normalized to  $T_0 \equiv [M_o c^2 / (r_g^2 \sigma_B)]^{1/4}$ , where  $\sigma_B$  is the Stefan-Boltzmann constant. The lower three curves are for a Novikov-Thorne disk, while the upper two are for an  $\epsilon = 1$  disk. The solid lines are without returning radiation, while the dotted lines include returning radiation. The dashed line shows the result of Cunningham (1976).

### 3.2. Emitted spectrum

The effective temperature is determined by the sum of the locally generated and returning flux. Figure 6 illustrates the effects discussed in §2, showing both how the intrinsic dissipation varies as a function of radius when there is a torque on the disk inner edge, and the total surface flux if one assumes that any incident radiation is absorbed. By comparing the curves for  $\Delta\epsilon = 0$  with the other curves, it is clear that the additional stress has two effects: the additional intrinsic dissipation creates a region at small radius where the effective temperature is rather higher than the disk could achieve otherwise; and returning radiation elevates the effective temperature at all radii, especially when  $a_*$  is near unity and  $\Delta\epsilon \sim 1$  or more.

Ideally, detailed atmosphere calculations should be performed in order to ascertain the predicted disk spectrum,

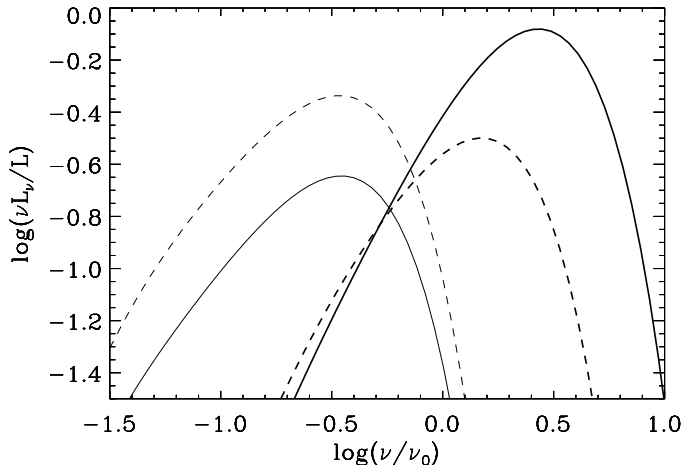


Fig. 7. Comparison of the spectra as a function of inclination angle for  $\epsilon = \epsilon_0$  (dashed lines) and  $\epsilon = \infty$  (solid lines). The other parameters are  $a_* = 0.998$ , and  $r_{out} = 500r_g$ . The heavy lines are for  $\mu = 0.01$  while the lighter lines are for  $\mu = 0.99$ . The frequency is scaled to  $\nu_0 \equiv (k/h) [L/(r_g^2 \sigma_B)]^{1/4}$ . The quantity  $L_\nu \equiv 4\pi D^2 F_\nu(\mu)$ , where  $F_\nu(\mu)$  is the flux seen by a Euclidean observer at distance  $D$  and angle  $\mu = \cos i$  relative to the accretion disk.

with the downgoing flux of returning radiation included in the upper boundary condition. Interesting effects might well be expected due to comparable amounts of heat arriving from above as from below. Pending the completion of that work, we make the much simpler assumption that the intensity at the surface of the disk is a blackbody at the local effective temperature, and isotropic in the outward half-sphere. With that assumption, Figures 7 and 8 show the predicted integrated spectrum for a variety of values of  $a_*$ ,  $\Delta\epsilon$ , and inclination (parameterized by  $\mu = \cos i$ ).

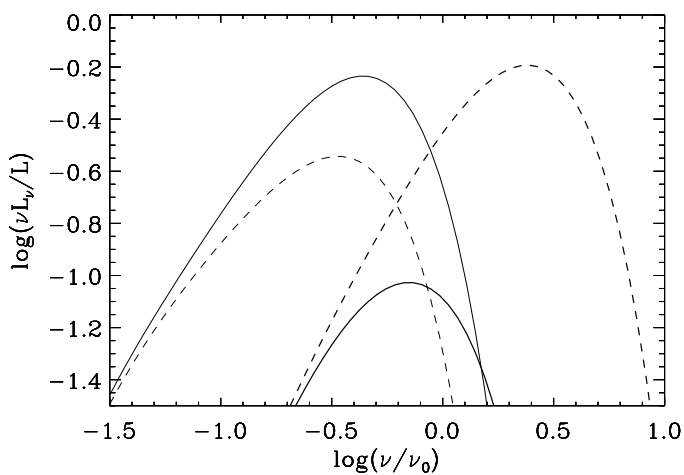


Fig. 8. Comparison of the spectra as a function of inclination angle for  $a_* = 0$  (solid lines) and  $a_* = 0.998$  (dashed lines) with  $\epsilon = 1$  and  $r_{out} = 500r_g$ . The heavier lines are for  $\mu = 0.01$ , while the lighter lines for  $\mu = 0.99$ . Units are the same as in Figure 7.

Figure 7 shows that for fixed luminosity and large spin, the efficiency of accretion can change the observed flux by

factors of a few at different inclination angles. The angle dependence of the flux depends strongly on frequency—the highest frequency radiation is concentrated towards the disk plane, while the lowest frequencies are radiated as  $\cos i$ . Figure 8 shows the dependence of the spectrum on black hole spin for fixed luminosity and efficiency. The relativistic effects are much stronger for the higher spin, hardening the edge-on spectrum and causing strong limb-brightening at the highest frequencies. In contrast, the disk around the Schwarzschild hole is limb-darkened at most frequencies, and, when face-on, is brighter by a factor of a few at the mid-range frequencies than the extreme Kerr hole. These effects may also impact the profiles of Fe K $\alpha$  emission lines. If their emissivity is proportional to the local flux, the enhanced flux in the inner rings of the disk strengthens the red wings of the lines when viewed more or less face-on. We plot the profiles of K $\alpha$  lines for disks with  $\Delta\epsilon = 0$  and  $\epsilon = \epsilon_{eq} = 0.293$  for  $a_* = 0$  and  $i = 30^\circ$  in Figure 9. Disks with higher spin have a smaller change in the shape of the iron line as a function of  $\epsilon$  because the returning radiation is much stronger and creates an emissivity profile very similar to the Novikov-Thorne profile. Magnetized accretion may also lead to enhanced coronal activity immediately above the plunging region (Krolik 1999); if so, this would provide a physical realization for models like those of Reynolds & Begelman (1997), which call for a source of hard X-rays on the system axis a few gravitational radii above the disk plane.

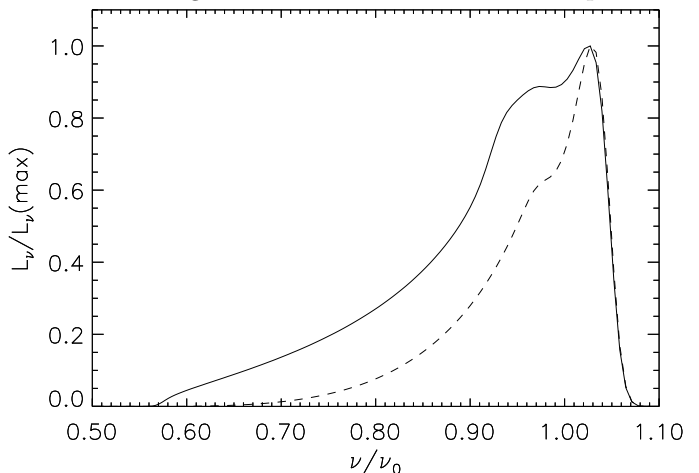


Fig. 9. Profiles of Fe K $\alpha$  lines for  $a_* = 0$ ,  $i = 30^\circ$ , and  $\epsilon = \epsilon_{eq} = 0.293$  (solid curve),  $\epsilon = \epsilon_0$  (dashed curve). Frequency is normalized to unshifted line frequency, and line amplitude is normalized to the line maximum.

### 3.3. Coordinated variations

When  $\Delta\epsilon$  is comparable to the ordinary efficiency, the inner rings of the disk radiate an amount of energy comparable to that radiated by all the rest of the disk. When, in addition,  $a_*$  is large enough that  $f_{ret}$  is significant, much of the light produced even at larger radii is reprocessed energy from the additional dissipation. If there are variations in that dissipation rate, they will be reproduced—in appropriate delays—in the reprocessed light. A prediction of this picture is therefore that fluctuations at a wide range of frequencies  $\nu$  should all be describable as driven by a single source. When the fluctuations in the returning flux are small compared to the mean local flux (combining both the intrinsic and the mean returning flux), the

relation between input and output may be written as the linear convolution

$$\delta L_\nu(t) = \int d\tau \Psi_\nu(\tau) \delta L_c(t - \tau), \quad (19)$$

where  $\delta L_c(t)$  is the history of fluctuations in the intrinsic output near  $r_{ms}$  and  $\Psi_\nu$  is a frequency-specific “response function”<sup>1</sup> that describes the distribution of relevant light-travel times. Note, however, that if there is a corona at small radii that receives a significant fraction of the total dissipation (indeed, such a corona might receive much of the extra accretion energy: Krolik 1999), it will also drive fluctuations in the output of the outer disk in very much the same manner, and with a substantially identical response function.

The response function  $\Psi_\nu(\tau)$  is also predicted by this model. To compute this function we make several simplifying approximations: that all the returning radiation is absorbed; that it is reradiated in a spectrum that is locally blackbody and isotropic in the outer half-sphere; and that the radii of interest are far enough out in the disk that relativistic effects may be ignored. Then

$$\Psi_\nu \simeq \frac{f_{\text{ret}} \mu r_* h \nu^3}{2cL_*} \int_{r_1}^{r_2} dr \frac{r^{3/4}}{e^{r^{3/4}} + e^{-r^{3/4}} - 2} \times \left[ 1 - \mu^2 - (c\tau/r - 1)^2 \right]^{-1/2}, \quad (20)$$

where radius  $r$  and  $c\tau$  are measured in units of  $r_*$ , the radius at which  $h\nu = kT$  when the flux takes its mean value,  $r_{in}$  is the innermost radius at which the returning flux is  $\propto r^{-3}$ ,  $r_1 = \max[r_{in}, c\tau/(1 - \sqrt{1 - \mu^2})]$ ,  $r_2 = c\tau/(1 - \sqrt{1 - \mu^2})$ , and  $\mu$  is the cosine of the inclination angle. The characteristic radius  $r_*$  is given by

$$r_* = \left( \frac{L_* r_{in} k^4}{4\pi\sigma h^4 \nu^4} \right)^{1/3}, \quad (21)$$

where  $k$  is the Boltzmann constant,  $\sigma$  is the Stefan-Boltzmann constant, and  $L_*$  is the mean value of the luminosity emitted by the portion of the disk whose emissivity is  $\propto r^{-3}$ .

Some sample response functions are illustrated in Figure 10. All of the curves have significant tails extending out to  $\sim 10r_*/c$ , and, almost independent of inclination angle, the “half-response time” (in the sense of  $\int d\tau \Psi_\nu$ ) occurs at  $\tau \simeq 3r_*/c$ . However, the peak in the response function becomes sharper and moves to smaller multiples of  $r_*/c$  as the inclination angle increases. Two effects account for this behavior. The tails are due to the fact that the temperature declines only as  $r^{-3/4}$ , so that the Wien cut-off sets in relatively slowly. The sharp peaks at small lag exhibited by disks with larger inclination angle are due to the significant amount of disk surface that lies close to the line of sight for those viewing angles.

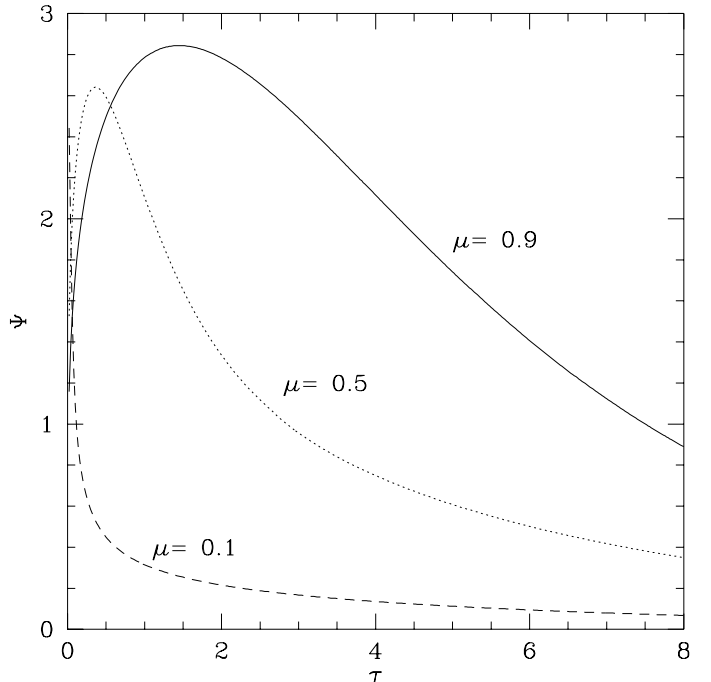


Fig. 10. Plot of continuum response  $\Psi_\nu$  as a function of lag for different inclinations.  $\Psi_\nu$  is in units of  $f_{\text{ret}} r_* h \nu^3 / (2cL_*)$  and  $\tau$  is in units of  $r_*/c$ .

### 3.4. Polarization

In fact, the inner rings of realistic disks, whether in AGN or Galactic black holes, are likely to be scattering-dominated, so that their albedo to the returning radiation will be significantly greater than zero. The scattered light may then be polarized.

As discussed in §2.2, the maximum altitude  $H$  above the disk plane achieved by any photon that ultimately returns to the disk cannot be much greater than a few gravitational radii. If the disk flare is small (see §3.6 for further discussion), the returning photons striking the disk at radius  $r$  must then arrive from an angle  $\simeq H/r \ll 1$  from the disk equator. When electron scattering is the dominant scattering opacity (as is nearly always the case), only those photons polarized parallel to the disk normal can scatter to outgoing directions near the equatorial plane but perpendicular to the original photon direction. The result is that disks viewed obliquely should acquire a small amount of polarization parallel to the disk axis, especially at the high frequencies produced predominantly in the inner rings.

To quantify this suggestion, we have computed the disk spectrum, treating the locally generated radiation as a blackbody, and assuming the returning radiation is scattered off a semi-infinite electron scattering atmosphere (Chandrasekhar 1960). We assume the locally generated disk flux has either (1) the polarization of a semi-infinite electron scattering atmosphere (Chandrasekhar 1960) or (2) is unpolarized. The true polarization will be modified by Faraday rotation due to magnetic fields in the disk’s atmosphere and absorption/emission (Agol, Blaes, & Ionescu-Zanetti 1998), but the true answer will likely lie between our two assumptions. Figure 11 shows the flux, polarization, and polarization angle computed under

<sup>1</sup>We use the term “response function” to avoid confusion with the relativistic “transfer function”.

these two assumptions. The spectrum is much broader than would be predicted by complete absorption, and returning radiation can cause a sharp rise in polarization towards the highest frequencies. There is a rotation in the polarization angle since the scattered returning radiation tends to be polarized perpendicular to the disk plane, while the locally generated radiation is polarized parallel to the disk plane. Whichever component dominates the flux at a given frequency determines the strength and angle of the polarization. We have included all relativistic effects that modify the final polarization angle (Laor, Netzer, & Piran 1990, Agol 1997). The returning fraction is largest for photons generated in the inner region of the disk; consequently, the highest frequencies have the largest scattered fraction and thus the highest polarization. In addition, the inner parts of the disk are strongly blueshifted, and the returning radiation is (weakly) Compton up-scattered by the bulk motion of the disk.

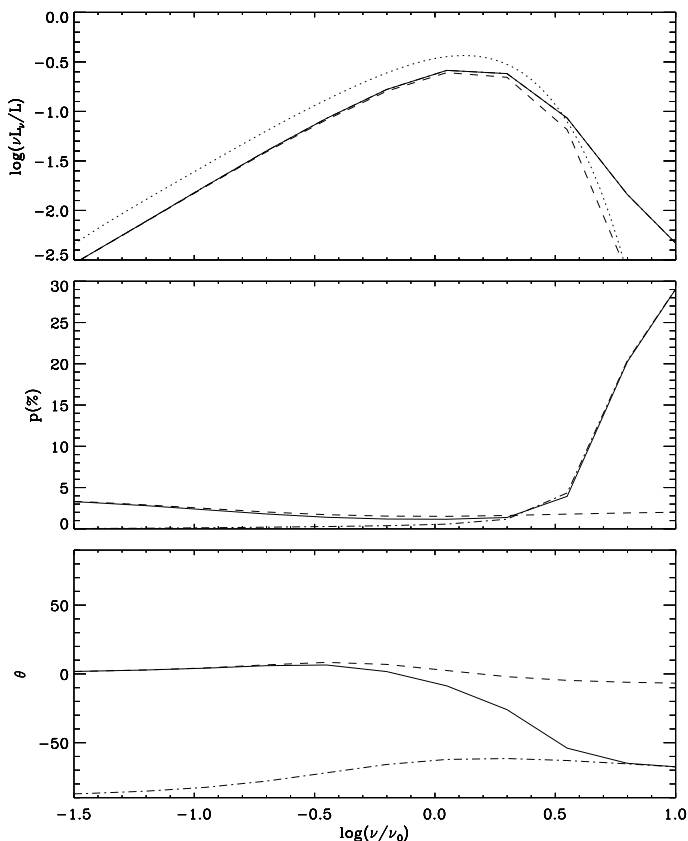


Fig. 11. Flux, polarization, and polarization angle as a function of frequency for a disk viewed with an inclination of  $\mu = \cos i = 0.2$ , with  $a = 0.998$ ,  $\Delta\epsilon = 1$ . The dashed curves are for no returning radiation; dashed-dot for returning radiation, but unpolarized locally generated flux; the solid curves are for returning radiation plus polarized locally generated flux; and the dotted line in the top panel shows the flux computed assuming complete absorption, as in §3.2. The polarization angle,  $\theta$ , is zero for  $\mathbf{E}$  parallel to the disk plane. The units are defined in Figure 7.

### 3.5. Bolometric Limb-brightening

For a Newtonian disk, foreshortening causes limb-darkening proportional to  $\mu = \cos i$ , where  $i = 0$  is a face-on disk. Relativistic effects cause beaming and bending of

the radiation towards the equatorial plane, which decrease the limb-darkening for disks around black holes. For large  $a_*$  and  $\epsilon$ , the relativistic effects become so strong that a disk can actually become *limb-brightened*. In Figure 12 we show the bolometric disk flux as a function of inclination angle for the cases  $\epsilon = \infty$  (dashed line),  $\epsilon = 1$  (dotted line), and  $\epsilon = \epsilon_0$  (solid line) for  $a_* = 0.998$ . The limb-brightening is also dependent on frequency as shown in §3.2; in practice, determining this quantitatively will require a detailed disk atmosphere model.

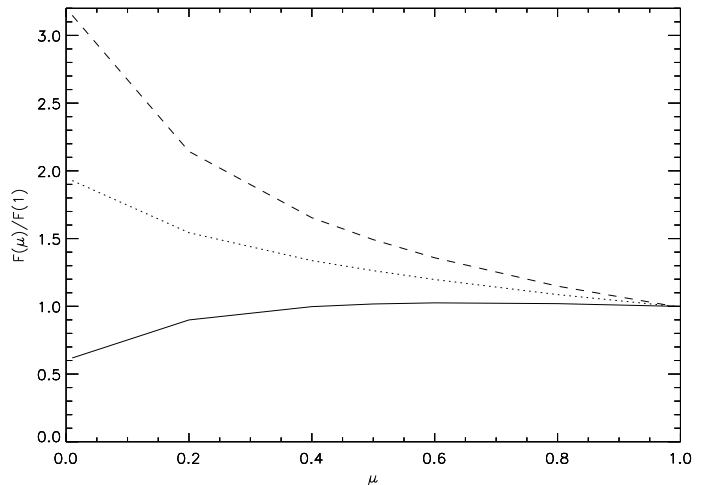


Fig. 12. Comparison of the bolometric limb-brightening of a disk for  $a_* = 0.998$  with  $\epsilon = \epsilon_0$  (solid line),  $\epsilon = 1$  (dotted line), and  $\epsilon = \infty$  (dashed line). The inclination angle,  $\mu = \cos i$  is edge-on for  $\mu = 0$  and face-on for  $\mu = 1$ .

### 3.6. Geometrical thickness of the disk

When the accretion rate is greater than a small fraction of the Eddington rate, the innermost regions of accretion disks are expected to be supported against the vertical component of gravity by radiation (Shakura & Sunyaev 1973). In that case, the disk's vertical thickness is directly proportional to the ratio of the local radiation flux to the vertical component of gravity; that is,  $h \propto Fr^3/R_z$ , where  $R_z$  is the relativistic adjustment to the vertical gravity (Page & Thorne 1974; Abramowicz, Lanza, & Percival 1997). At radii large enough that the relativistic effects are small, but not so large as to no longer be in the radiation-dominated regime in a Novikov-Thorne disk,  $h$  should be constant. In the relativistic portion of the disk,  $h$  would shrink  $\propto R^{NT}/R_z$  if the stress at its inner edge were zero; additional dissipation, depending on its strength, could actually make the disk become somewhat thicker there (cf. equation 8). We plot some examples of  $h(r)$  in Figure 13. At the inner edge of the disk, the height of the disk is non-zero when there is a non-zero torque, so the thin-disk approximation is valid only if  $h(r_{ms}) \lesssim 0.1r_{ms}$ . This criterion can be translated into a limit on the extra luminosity due to the torque at the inner edge:

$$\frac{L}{L_{Edd}} < 0.1 \frac{2}{3x_{ms}} \left( x_{ms} C_{ms}^{-1/2} F_{ms}^2 - a^2 G_{ms} + a^2 C_{ms}^{1/2} \right), \quad (22)$$

where  $L = \Delta\epsilon \dot{M}_o c^2$ . This limiting luminosity is plotted in Figure 14. When  $\Delta\epsilon = 0$ , the thin disk approximation breaks down if  $h/r \gtrsim 0.1$  where  $h/r$  is maximum. This



limit can in turn be expressed as a limit on the luminosity  $\epsilon_0 \dot{M}_o c^2$ , which is also shown in Figure 14. The luminosity upper limit for the infinite efficiency disk is much smaller than for the Novikov-Thorne disk since  $h/r$  peaks at  $r_{ms}$ , while for the Novikov-Thorne disk  $h/r$  peaks at larger radius, where its magnitude is smaller [ $(h/r)_{max}$  occurs at  $r = 24r_g$  for  $a_* = 0$  and  $r = 7r_g$  for  $a_* = 1$ ]. If either  $\epsilon_0 \dot{M}_o c^2$  or  $\Delta\epsilon \dot{M}_o c^2$  exceeds their respective limits, then the thin-disk approximation breaks down. In addition, if  $h/r$  is small, then the approximation of a flat disk in the computation of the returning radiation will be appropriate. To treat the interesting cases where  $L \sim L_{Edd}$  will require a 2-D solution of the disk equations, which is beyond the scope of this work. The returning radiation will not affect the disk height since it diffuses through the disk on a thermal timescale, so there is no net flux due to returning radiation (unless the disk is warped).

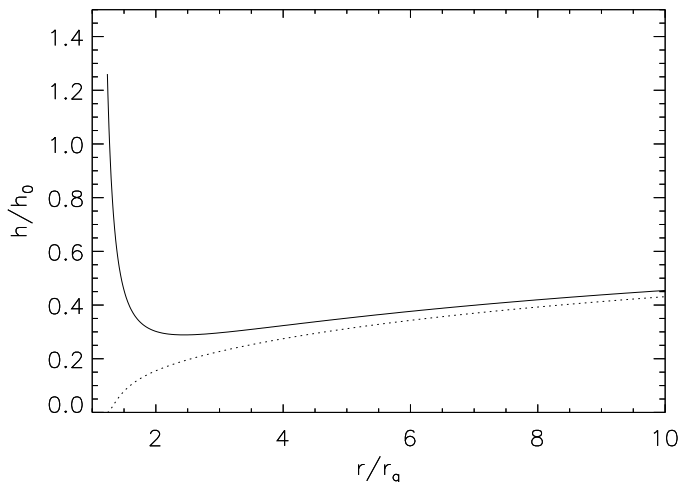


Fig. 13. Height of radiation pressure-supported disk vs. radius with  $\epsilon = \epsilon_0$  (dotted line) and  $\epsilon = 1$  (solid line) for  $a_* = 0.998$ . The height is normalized by  $h_0 \equiv 3\kappa \dot{M}_o / (8\pi c)$ .

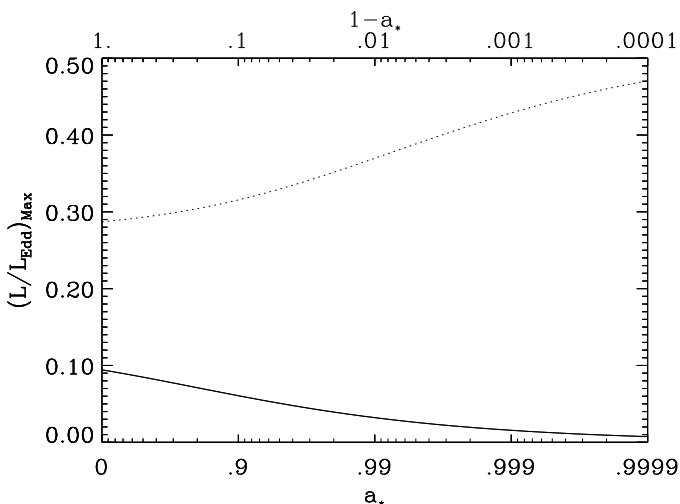


Fig. 14. Upper limit on the luminosity for thin-disk ( $h/r \lesssim 0.1$ ) approximation to be valid at  $r_{ms}$  for a radiation pressure-supported disk. Dotted line is for Novikov-

Thorne disk; solid line is for infinite-efficiency disk.

#### 4. CONCLUSIONS

We have generalized the equations for an azimuthally symmetric, geometrically thin, time-steady accretion disk around a black hole to include the effects of a torque operating at the inner boundary, taken to be at  $r_{ms}$ . Constant non-zero torque at  $r_{ms}$  causes several physical consequences that change the fundamental properties of the accretion flow:

1) The flux can be expressed as a sum of the usual Novikov & Thorne expression plus a part due to the torque which scales roughly as  $r^{-7/2}$ .

2) The accretion efficiency has a fundamental upper limit due to the second law of black hole dynamics for  $a_* < 0.36$ . For larger  $a_*$ , infinite efficiency is possible in principle.

3) The black hole spin can reach an equilibrium for  $a_* < 0.998$  since the angular momentum reaching the hole is smaller. Radiation can also exert a significant torque on the black hole, which changes the value of the equilibrium-spin efficiency. Above an efficiency of  $\epsilon = 0.36$ , the black hole must always be spun down.

4) Since the extra emissivity is peaked at the inner edge of the disk, if  $r_{ms}$  is small then gravity causes a large fraction of the radiation (up to 58%) to return to the accretion disk. The flux of returning radiation scales as  $r^{-3}$  at large radius. Up to 15% of the radiation can be captured by the black hole.

5) The extra heating within the disk will increase the height of the disk if it is radiation pressure-supported. This limits severely the luminosity at which the thin-disk approximation is appropriate.

6) Doppler beaming and relativistic bending are strongest in the inner parts of the accretion disk where the extra flux peaks, so that for large  $a_*$  and  $\epsilon$ , the disk will be limb-brightened.

These each have multiple observable consequences:

1) The extra surface brightness changes the locally radiated spectrum. Though the local surface brightness is usually not directly observable, it may be possible to map it using several devices: eclipse mapping (Baptista et al. 1998), although no eclipsing black hole X-ray binaries have been discovered yet; quasar microlensing (Agol & Krolik 1999); or reverberation mapping (Collier et al. 1999). If the Fe K $\alpha$  emissivity is proportional to the local dissipation, these effects can strengthen the red wing of the line, particularly when the spin is small. This effect may undercut the argument that lines with strong red wings came from disks around black holes with higher spin (e.g. Dabrowski et al. 1997).

Several authors have used the Novikov-Thorne model to fit the soft X-ray spectra of galactic black hole candidates. Their procedure was to estimate the effective radiating area required to emit the observed luminosity at the observed effective temperature. On the basis of these fits they inferred that some black holes have rather high spins because the effective radiating area of a Novikov-Thorne disk decreases with increasing spin (Zhang, Cui, & Chen 1997). However, for fixed spin and central mass, a disk with large  $\Delta\epsilon$  has a smaller effective radiating area than a Novikov-Thorne disk, mimicking the effect of greater spin.

2) The outer parts of accretion disks can be unstable to

warping due to irradiation from the center (Pringle 1996). The minimum radius for growth of small warps is proportional to  $\epsilon^{-2}$ ; if the efficiency is much higher than that of a standard disk, the minimum radius may be greatly shrunk. Limb-brightening increases the effective efficiency and therefore makes the linear growth more rapid; on the other hand, the corresponding relative decrease in intensity away from the central disk plane may weaken this effect in the non-linear regime.

3) Wavelength-dependent limb-brightening (or limb-darkening) introduces viewing angle-dependent biases into any flux-limited sample. This is a particularly strong effect in the context of quasar surveys because the number count distribution is so steep. A variety of distortions could occur in our view of what constitutes a “typical” quasar (cf. Krolik & Voit 1998).

4) Returning radiation can change the conditions for launching a radiation-driven disk wind (e.g. Murray et al. 1995). The returning radiation is reradiated locally, so the net vertical force depends on the frequency-averaged opacities of the downgoing and upgoing radiation fields. The radial component of the radiation force will be larger than for a standard disk due to the higher efficiency and limb brightening.

5) Returning radiation causes the various annuli to “communicate” on the light crossing timescale. Fluctuations of the flux at small radii will cause only slightly delayed fluctuations of the flux at larger radii, which emit at longer wavelengths. Indeed, exactly this sort of behavior is commonly seen in accreting black hole systems. For example, campaigns monitoring AGN have consistently found that continuum fluctuations are very nearly simultaneous all the way from  $\simeq 1300 \text{ \AA}$  to  $\simeq 5000 \text{ \AA}$  (Clavel et al. 1991; Korista et al. 1995; Wanders et al. 1997; Collier et al. 1998; O’Brien et al. 1998; Cutri et al. 1985). Comparing the upper bounds on any inter-band delays to the radial scales expected on the basis of conventional disk models, these observations have been interpreted as requiring a

coordinating signal group speed of at least  $\sim 0.1c$  (e.g., Krolik et al. 1991; Courvoisier & Clavel 1991; Collier et al. 1998).

6) The scattered component of returning radiation is highly polarized parallel to the disk axis at high frequencies. This polarization rise may be related to the observed sharp rises in several quasars (Koratkar et al. 1995, Impey et al. 1995). If the inner regions of the disk have a strong Lyman continuum in emission, then this scattered emission edge will appear as a strongly polarized, blueshifted emission edge in the spectrum. In an irradiated disk atmosphere there might be an additional effect: heating of the upper layers of the atmosphere can cause a temperature inversion, which changes the sense of the polarization. We leave all such detailed calculations to future work.

A question left unanswered by this work is what spin and efficiency we expect to be achieved by black holes in nature. That there is an upper limit on efficiency for an equilibrium spin means that a black hole with  $\epsilon > \epsilon_{eq}$  must be born with original spin, or must be spun up by accretion in which magnetic torques inside  $r_{ms}$  do not play an important role. In the supermassive black hole case, the spin may result from a merger. No one has computed the final spin of the resulting merger of two black holes; however, current approximate calculations indicate that the final spin could be quite large (Khanna et al. 1999). The strength of the torque at  $r_{ms}$  depends on the strength of the magnetic field in the accretion disk and the geometrical thickness of the flow, which in turn depend on the accretion rate. This dependence will be best addressed with numerical simulations of MHD accretion.

We would like to thank Roger Blandford, Doug Eardley, and Omer Blaes for helpful conversations. We would also like to thank the Institute for Theoretical Physics at U.C., Santa Barbara for its hospitality.

This work was partially supported by NASA Grant NAG 5-3929 and NSF Grant AST-9616922.

## APPENDIX

The function  $R_{ret}$  can be expressed as the sum of a part due to the Novikov & Thorne accretion rate, and a part due to the torque at the inner edge:

$$R_{ret}(\epsilon, a_*, r) = R_0(a_*, r) + R_\infty(a_*, r)\Delta\epsilon. \quad (1)$$

At large radius, these functions become constant, where we have fitted them with polynomials in  $x \equiv \log_{10}(1 - a_*)$ :

$$\begin{aligned} R_0(a_*, \infty) &= 0.0200 - 0.0360x + 0.0279x^2 + 0.00213x^3 - 0.00153x^4 - 0.000225x^5, \\ R_\infty(a_*, \infty) &= 0.594 - 0.199x - 0.116x^2 - 0.107x^3 - 0.0373x^4 - 0.00409x^5. \end{aligned} \quad (2)$$

TABLE 1  
COEFFICIENTS FOR FITS TO  $dM/dt$  AND  $dJ/dt$ .

fit	$a_0$	$a_1$	$a_2$	$a_3$	$a_4$	$a_5$	$a_6$
$10^4(dM/dt)_{rad}^0$	2.402	-11.63	10.87	-28.47	-17.30	-3.651	-0.2731
$10^4(dM/dt)_{rad}^\infty$	261.8	-600.9	449.7	554.9	224.9	41.28	2.885
$10^4(dJ/dt)_{rad}^0$	.5182	1.055	-5.149	3.707	2.347	.5455	.04527
$10^4(dJ/dt)_{rad}^\infty$	88.53	29.56	-29.19	-200.6	-128.1	-30.00	-2.475

The formulae are accurate to better 0.6% from  $a_* = 0$  to  $a_* = 0.9999$ .

For computing the spin evolution of an accreting black hole, it is useful to know  $(dJ/dt)_{rad} = (dJ/dt)_{rad}^0 + \Delta\epsilon(dJ/dt)_{rad}^\infty$  and  $(dM/dt)_{rad} = (dM/dt)_{rad}^0 + \Delta\epsilon(dM/dt)_{rad}^\infty$ . Note that  $(dM/dt)_{rad}^0 = M'_1 + \epsilon_0 M'_2$  and  $(dM/dt)_{rad}^\infty = M'_2$ , and likewise for  $J$ . We have fitted these with 6th order polynomials in  $x$ . The coefficients  $a_i$  of the fits ( $\sum_{i=0}^5 a_i x^i$ ) are given in table 1, where we have multiplied each  $a_i$  by  $10^4$ .

#### REFERENCES

- Abramowicz, M., Lanza, A. & Percival, M. 1997, ApJ 479, 179  
 Agol, E., 1997, PhD Thesis, University of California, Santa Barbara  
 Agol, E., Blaes, O., & Ionescu-Zanetti, C., 1998, MNRAS, 293, 1  
 Agol, E. & Krolik, J.H. 1999, ApJ, 507, 304  
 Balbus, S.A. & Hawley, J.F. 1998, Revs. Mod. Phys., 70, 1  
 Baptista, R. et al., 1998, MNRAS, 298, 1079  
 Blandford, R. D., 1998, in *AIP Conference Proceedings 431, Accretion Processes in Astrophysical Systems: Some Like it Hot! Eighth Astrophysics Conference, College Park, MD 1997*, Holt, S. S. & Kallman, T. R., eds., p. 43  
 Chandrasekhar, S., 1960, *Radiative Transfer* (New York: Dover Books)  
 Clavel, J. et al., 1991, ApJ, 366, 64  
 Collier, S. et al. 1998, ApJ, 500, 162  
 Collier, S., Horne, K., Wanders, I., & Peterson, B., 1999, MNRAS, 302, L24  
 Courvoisier, T. & Clavel, J. 1991, A. & A. 248, 389  
 Cunningham, C.T. 1976, ApJ 208, 534  
 Cutri, R. M.; Wisniewski, W. Z., Rieke, G. H., & Lebofsky, M. J., 1985, ApJ, 296, 423  
 Dabrowski, Y., et al., 1997, MNRAS, 288, L11  
 Gammie, C. 1999, ApJL, 522, in press  
 Impey, C. D., Malkan, M. A., Webb, W., & Petry, C. E., 1995, ApJ, 440, 80  
 Khanna, G., et al., 1999, gr-qc/9905081  
 King, A. R. & Lasota, J. P., 1977, A&A, 58, 175  
 Koratkar, A., Antonucci, R. R. J., Goodrich, R. W., Bushouse, H., & Kinney, A. L., 1995, ApJ, 450, 501  
 Korista, K.T. et al. 1995, ApJSS, 97, 285  
 Krolik, J.H. 1999, ApJ, 515, L73  
 Krolik, J.H., Horne, K.D., Kallman, T.R., Malkan, M.A., Edelson, R.A., and Kriss, G.A. 1991, ApJ, 371, 541  
 Krolik, J.H. & Voit, G.M. 1998, ApJ, 497, L5  
 Laor, A., Netzer, H., & Piran, T., 1990, MNRAS, 242, 560  
 Murray, N., Chiang, J., Grossman, S.A. & Voit, G.M. 1995, ApJ, 451, 498  
 Novikov, I.D. & Thorne, K.S. 1973, in *Black Holes*, eds. C. De Witt and B. De Witt (New York: Gordon & Breach), p. 343  
 O'Brien, P.T. et al. 1998, ApJ, 509, 163  
 Page, D. & Thorne, K.S. 1974, ApJ, 191, 499  
 Popham, R. & Narayan, R., 1993, ApJ, 442, 337  
 Pringle, J.E. 1996, MNRAS, 281, 357  
 Reynolds, C. & Begelman, M. 1997, ApJ, 488, 109  
 Ruffini, R. & Wilson, J.R., 1975, Physical Review D (Particles and Fields), 12, 2959  
 Shakura, N.I. & Sunyaev, R.A. 1973, A&A 24, 337  
 Thorne, K.S. 1974, ApJ, 191, 507  
 Wanders, I. et al. 1997, ApJSS, 113, 69  
 Zhang, S. N., Cui, W., Chen, W., 1997, ApJ, 482, L155